

Theory of the hourglass dispersion of magnetic excitations in high- T_c cuprates

Roland Zeyher¹

¹*Max-Planck-Institut für Festkörperforschung, Heisenbergstrasse 1, D-70569 Stuttgart, Germany*

(Dated: November 9, 2018)

A theory for the dispersion of collective magnetic excitations in superconducting cuprates is presented with the aim to cover both high and low doping regimes. Besides of spin fluctuations describable in the random phase approximation (RPA) we allow for local spin rotations within a mode-coupling theory. At low temperatures and moderately large correlation lengths we obtain two branches of excitations which disperse up- and downwards exhibiting the hourglass behavior observed experimentally at intermediate dopings. At large and small dopings our theory essentially reduces to the RPA and spin wave theory, respectively.

PACS numbers: 75.40.Gb, 74.25.Ha, 74.72.-h

The low-temperature magnetic response of many high- T_c superconductors is characterized by a resonant mode inside the superconducting gap around the antiferromagnetic wave vector \mathbf{Q} . This collective mode manifests itself as a single peak at \mathbf{Q} which splits into two peaks dispersing up- and downwards in frequency away from \mathbf{Q} . This unusual dispersion resembles the shape of a hourglass[1, 2]. Theories to explain this phenomena use either a more local[3] or an itinerant[4, 5] description of the magnetism. The second approach considers particle-hole excitations with spin flips which interact within the random phase approximation (RPA) forming a dispersing bound state in the superconducting gap. This approach yields only one branch of excitations below the Stoner continuum whereas it has been established recently that the lower branch, the center of the hourglass as well as part of the upper branch lie below this continuum in the gapped region[1]. A more theoretical argument for the incompleteness of a RPA description comes from the fact that different spin directions do not mix as a function of time in this approximation which excludes local rotations of spins known from spin wave theory. Below we will present a theory which contains both spin wave theory and RPA as special cases. At intermediate dopings we will show that both RPA and spin wave like spin fluctuations are important and produce the two branches of the hourglass dispersion.

We consider the t - J model[6] with the Hamiltonian H ,

$$H = \sum_{\mathbf{k}\sigma} \epsilon(\mathbf{k}) \tilde{c}_{\mathbf{k}\sigma}^\dagger \tilde{c}_{\mathbf{k}\sigma} + \frac{1}{2} \sum_{\mathbf{k}} J(\mathbf{k}) \mathbf{S}_{\mathbf{k}} \mathbf{S}_{-\mathbf{k}}. \quad (1)$$

$\tilde{c}_{\mathbf{k}\sigma}^\dagger, \tilde{c}_{\mathbf{k}\sigma}$ are creation and annihilation operators, respectively, for electrons with momentum \mathbf{k} and spin projection σ excluding any double occupancies of sites. $\mathbf{S}_{\mathbf{k}}$ are spin operators in momentum space, $\epsilon(\mathbf{k})$ and $J(\mathbf{k})$ are the bare electron dispersion and the Fourier transform of the Heisenberg coupling, respectively. A useful approximation for H , used in the following, is obtained by taking the large N limit of the t - J model, where $\epsilon(\mathbf{k})$ describes a renormalized dispersion of quasi-particles and

the fermionic operators can be treated as usual creation and annihilation operators.

In the following we are interested in the time evolution of the spin operator $\mathbf{S}_{\mathbf{k}} = 1/2 \sum_{\mathbf{q}} \mathbf{A}(\mathbf{k}, \mathbf{q})$,

$$\mathbf{A}(\mathbf{k}, \mathbf{q}) = \sum_{\alpha, \beta} c_{\mathbf{k}+\mathbf{q}\alpha}^\dagger \boldsymbol{\sigma}_{\alpha\beta} c_{\mathbf{q}\beta}, \quad (2)$$

where $\boldsymbol{\sigma}$ denotes the vector of the three Pauli matrices. It obeys the equation of motion

$$\frac{\partial \mathbf{A}}{\partial t} = i(\mathcal{L}_0 + \mathcal{L}_1) \mathbf{A}, \quad (3)$$

with

$$\begin{aligned} \mathcal{L}_0 \mathbf{A}(\mathbf{k}, \mathbf{q}) &= (\epsilon(\mathbf{k} + \mathbf{q}) - \epsilon(\mathbf{q})) \mathbf{A}(\mathbf{k}, \mathbf{q}) \\ &+ J(\mathbf{k})(f(\mathbf{q}) - f(\mathbf{k} + \mathbf{q})) \mathbf{S}_{\mathbf{k}}, \end{aligned} \quad (4)$$

$$\begin{aligned} \mathcal{L}_1 \mathbf{A}(\mathbf{k}, \mathbf{q}) &= -\frac{i}{2} \sum_{\mathbf{k}'} J(\mathbf{k}') \cdot \\ &\left(\mathbf{S}_{\mathbf{k}'} \times (\mathbf{A}(\mathbf{k} - \mathbf{k}', \mathbf{q}) + \mathbf{A}(\mathbf{k} - \mathbf{k}', \mathbf{k}' + \mathbf{q})) \right). \end{aligned} \quad (5)$$

$f(\mathbf{k})$ is equal to $\langle c_{\mathbf{k}\sigma}^\dagger c_{\mathbf{k}\sigma} \rangle$, where $\langle \dots \rangle$ denotes the thermodynamic expectation value, and \times stands for the vector product. Since we are only interested in the spin response we have dropped terms on the right-hand side of Eq.(5) which involve fluctuations in the density. We also dropped an overall prefactor denoting the number of primitive cells. The unperturbed Liouville operator \mathcal{L}_0 describes the time evolution of the system in the RPA. From its explicit expression in Eq.(4) follows that it does not mix different cartesian components of the spin operators. In contrast to that the time evolution described by \mathcal{L}_1 involves product states of spin operators, mixes different spin components and thus can describe rotations of spins due to fluctuating fields.

The spin susceptibility $\chi(\mathbf{k}, z)$ can conveniently be calculated from the associated Kubo relaxation function

$\Phi(\mathbf{k}, z) = (\chi(\mathbf{k}) - \chi(\mathbf{k}, z))/z$ where z is a complex frequency and $\chi(\mathbf{k})$ is equal to $\chi(\mathbf{k}, z = 0)$. Due to the rotational invariance in spin space we may assume that χ , M etc. always refer to the z -direction. Using the Mori formalism Φ can be written as[7]

$$\Phi(\mathbf{k}, z) = \frac{\chi(\mathbf{k})}{z + M^{\text{RPA}}(\mathbf{k}, z) + M(\mathbf{k}, z)}. \quad (6)$$

The first memory kernel $M^{\text{RPA}}(\mathbf{k}, z)$ describes the time evolution of spin operators by \mathcal{L}_0 . According to Eq.(4) the direction of the spin operators is conserved and they remain always linear in the operators \mathbf{A} . Eliminating the \mathbf{A} operators in the equation of motion in favor of the original \mathbf{S} operators yields an explicit expression for M^{RPA} which may be expressed in terms of the RPA spin susceptibility $\chi^{\text{RPA}}(\mathbf{k}, z)$,

$$M^{\text{RPA}}(\mathbf{k}, z) = z\chi^{\text{RPA}}(\mathbf{k}, z)/(\chi^{\text{RPA}}(\mathbf{k}) - \chi^{\text{RPA}}(\mathbf{k}, z)), \quad (7)$$

with

$$1/\chi^{\text{RPA}}(\mathbf{k}, \omega) = 1/\chi^{(0)}(\mathbf{k}, \omega) + J(\mathbf{k}), \quad (8)$$

$\chi^{(0)}(\mathbf{k}, \omega)$ is the free susceptibility.

The second memory contribution $M(\mathbf{k}, z)$ is due to the time evolution of single spin operators \mathbf{S} into product states of spin operators described by \mathcal{L}_1 . Using the mode-coupling assumption and performing the analytic continuation $z \rightarrow \omega + i\eta$, we obtain for the imaginary part of M , denoted by M'' ,

$$M''(\mathbf{k}, \omega) = \sum_{\mathbf{k}'} (J(\mathbf{k}') - J(\mathbf{k} - \mathbf{k}'))^2 D''(\mathbf{k}, \mathbf{k}', \omega) / (\omega \chi(\mathbf{k})), \quad (9)$$

$$D''(\mathbf{k}, \mathbf{k}', \omega) = \pi \int d\omega' A(\mathbf{k} - \mathbf{k}', \omega - \omega') A(\mathbf{k}', \omega') (b(\omega') - b(\omega' - \omega)). \quad (10)$$

A is the spectral function of the spin propagator and $b(\omega)$ the Bose function.

SMALL CORRELATION LENGTHS

In the case of small antiferromagnetic correlation lengths ξ , corresponding to the overdoped regime, the RPA should be a reasonable approximation for the spin susceptibility. The dashed line in Fig. 1 shows the imaginary part of $\chi^{\text{RPA}}(\mathbf{Q}, \omega)$ for $\mathbf{Q} = (\pi, \pi)$ using the parameters t and U in Table I of Ref.[4] and a chemical potential corresponding to the doping $\delta = 0.20$. The energy unit is 1 eV in the following and lengths are measured in units of the lattice constant a of the square lattice. The superconducting order parameter is $\Delta(\mathbf{k}) = \Delta(\cos k_x - \cos k_y)/2$ with $\Delta = 0.029$, J equal to 0.135 and $\eta = 0.004$. The dashed line in Fig. 1 illustrates that most of the spectral

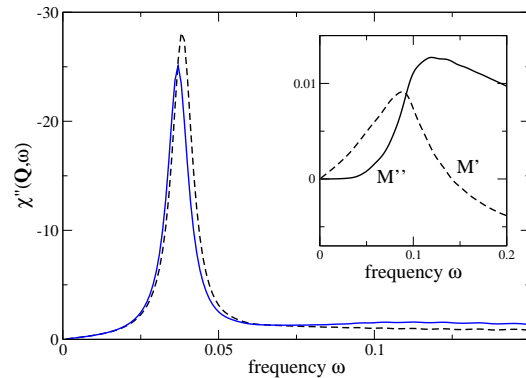


FIG. 1: $\chi''(\mathbf{Q}, \omega)$ without (dashed line) and with (solid line) memory function M for a doping $\delta = 0.20$ and $T = 0$. The dashed curve corresponds to the RPA. Inset: real part M' and imaginary part M'' of $M(\mathbf{Q}, \omega)$.

weight resides in the bound state at the energy 0.038 and that only a small part of it has been left in the continuum at higher energies. Away from (π, π) the dashed curve in Fig.1 does not change dramatically as long as the bound state lies still in the gapped region. Entering the particle-hole continuum by going further away from (π, π) destroys the bound state and most of the spectral weight shifts to high energies of the order of t . The parameters used in Fig. 1 yield $\xi \sim 0.78$. For such a small ξ practically all momenta in the sum over momenta in Eq.(9) contribute substantially which means that M'' is mainly determined by contributions away from the small region around (π, π) so that the bound state and its low-energy scale is rather irrelevant for M . This is confirmed by an explicit calculation of M using RPA results for the various quantities in Eq.(9). The result is shown in the inset of Fig. 1 for $T=0$. M'' (solid line) is structureless except at small energies where it vanishes rapidly due to the smallness of A in this region and the cutoff ω for the integration over ω' in Eq.(10) due to the bosonic factors. Taking M into account in Eq.(6) yields the solid line in Fig. 1 which differs only marginally from the dashed line. This shows that at short correlation lengths the RPA result for χ'' is essentially correct and that the correction M to M^{RPA} is rather small. The underlying physical picture is that the momentary local axis of preferred spin directions fluctuates very rapidly due to the random forces induced by \mathcal{L}_1 . The spectrum of these forces is given by M'' and characterized by the large energy scale t in agreement with the inset of Fig. 1.

LARGE CORRELATION LENGTHS

For large ξ the spectral function $A(\mathbf{k}', \omega')$ is strongly peaked at $\mathbf{k}' = \mathbf{Q}$. This means that the integration over \mathbf{k}' in Eq.(9) is restricted to momenta near $\mathbf{0}$ or near

\mathbf{Q} . Since we are interested in external momenta $\mathbf{k} \sim \mathbf{Q}$ the momentum of one of the two spectral functions in Eq.(10) is small. Due to spin conservation this spectral function describes spin diffusion and is mainly restricted to small values of ω' . As a result one may neglect the small frequency transfer in the second spectral function in Eq.(10). Taking also the real part of M into account we obtain from Eqs.(9) and (10),

$$M(\mathbf{k}, \omega) = -\omega^2(\mathbf{k})\Phi(\mathbf{Q}, \omega)/\chi(\mathbf{Q}), \quad (11)$$

with

$$\omega^2(\mathbf{k}) = \frac{2}{\chi(\mathbf{k})} \sum_{\mathbf{q}} (J(\mathbf{q}) - J(\mathbf{k} - \mathbf{q}))^2 \langle S_{\mathbf{k}-\mathbf{q}} S_{\mathbf{q}-\mathbf{k}} \rangle \chi(\mathbf{q}), \quad (12)$$

and the equal-time correlation function

$$\langle S_{\mathbf{k}} S_{-\mathbf{k}} \rangle = \int d\omega b(\omega) A(\mathbf{k}, \omega). \quad (13)$$

In deriving Eq.(11) we used the fact that the two memory functions in Eq.(6) depend for our parameters only slowly on momentum around the wave vector \mathbf{Q} so that the combination Φ/χ on the right-hand side of Eq.(11) may be evaluated at \mathbf{Q} . The sum over \mathbf{q} in Eq.(12) runs over half of the Brillouin zone centered around \mathbf{Q} . The evaluation of the above expressions using the RPA encounters a problem: ξ , calculated in the RPA, is in the optimal and moderately underdoped region around one or smaller and increases substantially only near the transition to the antiferromagnetic state in disagreement with the experiment. For instance, we have for $\delta = 0.12$ $\xi \sim 0.8$, Ref.[5] $\xi \sim 0.6$ using quite different parameter values, whereas the experimental values for ξ are larger by about a factor 5 or more[8]. Since this large discrepancy would affect severely the momentum sum in Eq.(12) we prefer to use a realistic $\chi(\mathbf{k})$ as input in calculating M and write $\chi(\mathbf{k}) = \chi(\mathbf{Q})/(1 + \xi^2(\Delta\mathbf{k})^2)$ for $\Delta\mathbf{k} \equiv \mathbf{k} - \mathbf{Q} \sim 0$ considering ξ as a parameter to be determined from experiment.

It is instructive to study the frequency dependence of the denominator of Eq.(6). In order to describe a slightly underdoped case we choose the same parameters as in Fig. 1, a chemical potential corresponding to $\delta = 0.12$, $\xi = 5$, and the cutoff $1/\xi$ for the sum over \mathbf{q} in Eq.(12). The solid and dotted line in Fig. 2 show $1 + M'^{\text{RPA}}(\mathbf{k}, \omega)/\omega$ for $H=0.5$ and 0.38 , respectively, writing $\mathbf{k} = (H, 0.5)2\pi$. This quantity is practically independent of momentum, increases monotonically with ω and is zero at the RPA resonance energy $\omega_R \sim 0.038$. The dashed and dash-dotted lines in Fig. 2 show $-M'(\mathbf{k}, \omega)/\omega$ for the same momenta. These curves resemble the real part of an oscillator located at ω_R with an oscillator strength being very small at $\Delta\mathbf{k} \equiv \mathbf{k} - \mathbf{Q} = 0$ and strongly increasing with $|\Delta\mathbf{k}|$. The poles of Eq.(6) are given by the common points of the two curves denoted by squares and circles. Since the common point at

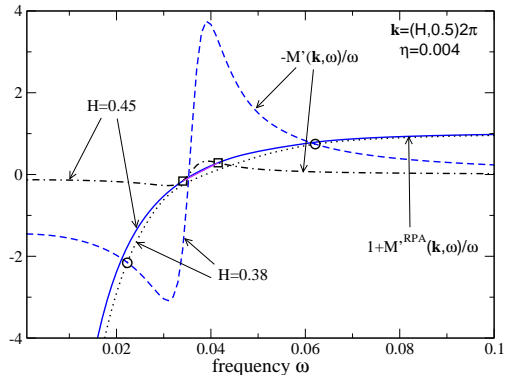


FIG. 2: (color online) $1 + M'^{\text{RPA}}(\mathbf{Q}, \omega)/\omega$ (solid and dotted lines) and $-M'(\mathbf{Q}, \omega)/\omega$ (dash-dotted and dashed lines) as a function of frequency for two momenta H . Squares and circles denote poles of $\chi(\mathbf{k}, \omega)$.

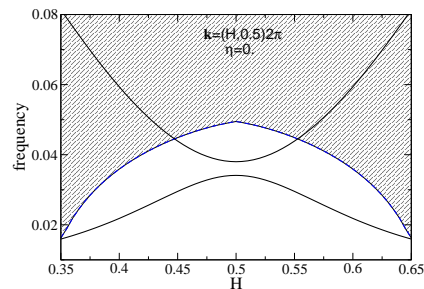


FIG. 3: (color online) Position of the poles of $\chi(\mathbf{k}, \omega)$ as a function of momentum. The shadowed region marks the particle-hole continuum.

$\omega = \omega_R$ (not shown in Fig. 2) has vanishing pole strength there are two branches of collective spin excitations. For vanishing damping η their dispersion is shown in Fig. 3 by solid lines. They approximately touch each other at $\Delta\mathbf{k} = 0$ and disperse up- and downwards with increasing $|\Delta\mathbf{k}|$. For not too large $|\Delta\mathbf{k}|$ both branches lie below the continuum in agreement with experiment[1]. Performing the calculation in the normal state at $T = T_c$ the solid and dotted lines in Fig. 2 lie everywhere above zero but the solid and dashed and also the dotted and dash-dotted lines have still one common point at larger frequencies. In this case only the upper but not the lower branch exists in agreement with experiment[2]. At very low dopings $M^{\text{RPA}} \rightarrow 0$ due to the constraint and the pole condition $\omega + M'(\mathbf{k}, \omega)$ yields in the presence of long-range order the correct spin wave dispersion[7].

Several prerequisites are necessary to obtain the above hourglass dispersion for spin excitations. There must exist two different kinds of spin excitations to account for the two branches. The first one are RPA spin fluctuations where all induced spin moments have the same direction. They may be characterized by the fact that

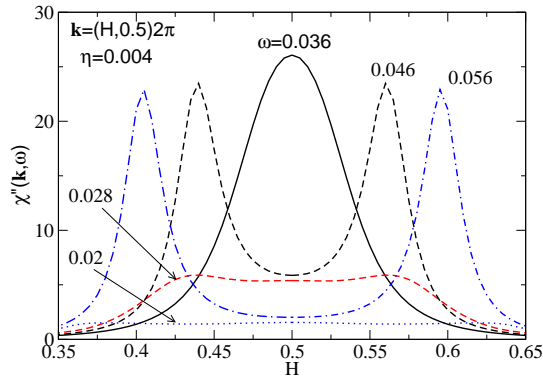


FIG. 4: (color online) Imaginary part of the spin susceptibility at zero temperature as a function of momentum for different frequencies.

the internal fields induced by the Heisenberg interaction conserves frequency, momentum and spin direction which is a direct consequence of the one-mode behavior of \mathcal{L}_0 in Eq.(4). The second one are local rotations of spins under the influence of \mathcal{L}_1 in Eq.(5). In this case a spin in z direction acquires in its time evolution also a component in x direction due to the presence of a spin fluctuation in y direction. The pure form of the two kind of spin excitations are obtained for $M = 0$ and $M^{\text{RPA}} = 0$, respectively, and are realized approximately at large and small dopings. In the hourglass regime M and M^{RPA} are of similar magnitude.

Another prerequisite for hourglass behavior is that ξ is substantially larger than 1. Only then is the momentum integration in Eq.(9) restricted to the resonance and the spin diffusion modes yielding oscillator-like behavior of M near ω_R . The up- and downwards dispersion and their approximate degeneracy at \mathbf{Q} is mainly determined by $\omega^2(\mathbf{k})$, which according to Eq.(12) is roughly proportional to $\langle S_{\Delta\mathbf{k}} S_{-\Delta\mathbf{k}} \rangle (\xi^{-2} + (\Delta\mathbf{k})^2)$. The first factor tends to zero at low temperatures for $\Delta\mathbf{k} \rightarrow 0$ and saturates at large $\Delta\mathbf{k}$. As a result $\omega^2(\mathbf{k})$ is very small at $\Delta\mathbf{k} = 0$ causing the approximate touching of the two branches at $\omega = \omega_R$ and $\Delta\mathbf{k} = 0$. With increasing $\Delta\mathbf{k}$ $\omega^2(\mathbf{k})$ increases strongly leading to a downward dispersion of the lower branch even if ω_R was practically dispersionless as in our case. According to Fig. 3 the upper branch increases at large $|\Delta\mathbf{k}|$ roughly as $0.6J|\Delta\mathbf{k}|$, i.e., with an effective spin wave velocity which is reduced by about a factor 2-3 compared to spin wave theory similar as in experiment[1, 2].

Using the same parameters as in Figs. 2 and 3 Fig. 4 shows χ'' as a function of H with the frequency as a parameter. As suggested by Fig. 3 χ'' exhibits a hourglass dispersion with intensities which are largest near ω_R and decay rather fast and slow towards lower and higher frequencies, respectively. Fig. 5 shows χ'' as a function of ω for a fixed H as a parameter. In agreement with Fig.

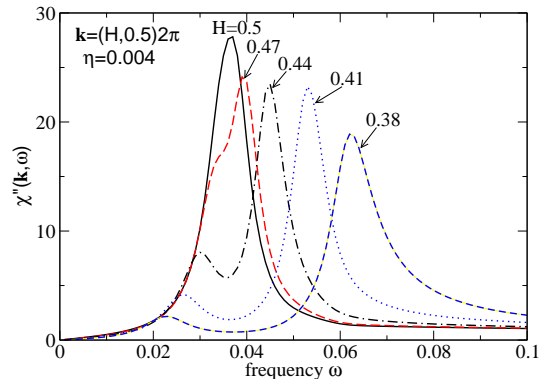


FIG. 5: (color online) Imaginary part of the spin susceptibility at zero temperature as a function of frequency for different momenta.

4 the strong peak at $H = 0.5$ splits into two peaks with decreasing H which disperse up- and downwards in frequency. The curve for $H = 0.5$ calculated for the small damping $\eta = 0.004$ has the shape of a Lorentzian. At smaller dampings this peak splits into a double peak due to the small gap between upper and lower branch shown in Fig. 3. For $M = 0$ only the lower, weaker peak is obtained.

In conclusion, we have shown that the memory function of the spin susceptibility contains in general two distinct contributions due to RPA-like and due to rotational spin fluctuations. The first one dominates at large, the second one at small dopings. At intermediate dopings both are of similar magnitude which leads to one upwards and one downwards dispersing branch of excitations. At low temperatures the two branches are approximately degenerate at \mathbf{Q} which explains, at least qualitatively, the observed hourglass dispersion at intermediate dopings.

The author is grateful to V. Hinkov, P. Horsch, D. Manske and H. Yamase for useful discussions.

-
- [1] B. Fauque et al., Phys. Rev. B **76**, 214512 (2007), and references therein.
 - [2] V. Hinkov et al., nature physics **3**, 780 (2007).
 - [3] I. Sega, P. Prelovsek, and J. Bonca, Phys. Rev. B **68**, 54524 (2003).
 - [4] M.R. Norman, Phys. Rev. B **63**, 92509 (2001).
 - [5] H. Yamase and W. Metzner, Phys. Rev. B **73**, 214517 (2006), and private communication.
 - [6] For a review, see M. Ogata and H. Fukuyama, Rep. Prog. Phys. **71**, 036501 (2008).
 - [7] D. Forster, "Hydrodynamic Fluctuations, Broken Symmetry, and Correlation Functions", W.A. Benjamin, Inc., Reading, Massachusetts (1975), chapter 9.
 - [8] P. Dai, H.A. Mook, R.D. Hunt, and F. Doğan, Phys. Rev. B **63**, 054525 (2001).